Journal of Solid State Chemistry 182 (2009) 1136–1141

Contents lists available at ScienceDirect

Journal of Solid State Chemistry

journal homepage: www.elsevier.com/locate/jssc

The polar mixed-valent lanthanum iron(II, III) sulfide $La_3Fe_{2-\delta}S_7$: Synthesis, crystal and electronic structure, ^{57}Fe Mößbauer spectra, magnetic susceptibility and electrical resistivity

Allison M. Mills [a], Daniel Bräunling [a], Helge Rosner [b], Walter Schnelle [b], C. Peter Sebastian [c], Rainer Pöttgen [c], Michael Ruck [a,*]

[a] Department of Chemistry and Food Chemistry, Dresden University of Technology, 01062 Dresden, Germany
[b] Max-Planck Institute for Chemical Physics of Solids, Nöthnitzer Str. 40, 01187 Dresden, Germany
[c] Institute for Inorganic and Analytical Chemistry, University of Münster, Corrensstr. 30/36 48149 Münster, Germany

ARTICLE INFO

Article history:
Received 20 November 2008
Received in revised form
21 January 2009
Accepted 26 January 2009
Available online 5 February 2009

Keywords:
Electronic structure
Mixed-valent compound
Moessbauer spectroscopy
One-dimensional conductor
Polar crystal structure

ABSTRACT

$La_3Fe_{2-\delta}S_7$ ($\delta = 0.042(6)$) was synthesized through a reaction of the elements in a LiCl/KCl flux at 970 K, and its structure was determined by single-crystal X-ray diffraction. The compound crystallizes in the polar hexagonal space group $P6_3$ with $a = 10.1906(6)$, $c = 5.9543(4)$ Å and $Z = 2$, and adopts the $Ce_6Al_{10/3}S_{14}$ structure type. The structure contains both octahedral and tetrahedral iron sites: one-dimensional rods of face-sharing FeS_6 octahedra run along the 6_3 screw axis of the cell; FeS_4 tetrahedra, all pointing in the same direction, are stacked along the threefold rotation axes. The iron-centered polyhedra are linked by lanthanum atoms, which are coordinated by [7+1] sulfur atoms in a bicapped trigonal prismatic arrangement. ^{57}Fe Mößbauer spectroscopy confirms that Fe^{III} and Fe^{II} cations occupy the tetrahedral and octahedral iron sites, respectively. Magnetic susceptibility data indicate an antiferromagnetic transition at $T_N \approx 155$ K. Density functional band structure calculations within the local density approximation reveal two covalent Fe–S subsystems within the compound that mix only weakly. A large anisotropy is indicated by bands that disperse predominantly along the hexagonal axis. The electronic band structure suggests pseudo-one-dimensional metallic conductivity along the rods of face-sharing FeS_6 octahedra. However, due to the defects on the Fe^{II} positions, $La_3Fe_{2-\delta}S_7$ shows an activated conducting behavior.

1. Introduction

A series of rare-earth iron sulfides initially described with the formula "R_4FeS_7" (R = La–Nd) was discovered in an early survey of the ternary system. Hexagonal cell parameters, determined from X-ray powder diffraction patterns, were reported at the time [1], and it was later recognized that the compounds adopt the $Ce_6Al_{10/3}S_{14}$ structure type (space group $P6_3$) [2]. Recently, a single-crystal structure determination of the cerium iron sulfide confirmed the structure type and revealed that the actual formula of the series is $R_3Fe_2S_7$ [3]. In these mixed-valent compounds, Fe^{II} and Fe^{III} cations occupy octahedral and tetrahedral sites, respectively. Stacks of FeS_4 tetrahedra and chains of face-sharing FeS_6 octahedra, both propagating in the [001] direction, are separated by trivalent rare-earth cations. Since the crystal structure is distinctly one-dimensional in character, anisotropic physical properties are expected for $R_3Fe_2S_7$. In light of the interesting phenomena exhibited by other compounds containing chains of iron–sulfur polyhedra, for example, magnetoresistance and spin-glass-like behavior in $BaFe_2S_3$ [4], a reinvestigation of the synthesis, structure and properties of the $R_3Fe_2S_7$ series appeared to be desirable.

The starting point for the present study is a detailed examination of the first member of the series, $La_3Fe_2S_7$. The absence of f electrons on the La^{III} cation entails that the magnetic properties of $La_3Fe_2S_7$ are determined solely by the iron cations, making this a useful model compound to which the other $R_3Fe_2S_7$ members can be compared. A neutron diffraction study showed that the magnetic structure of $La_3Fe_2S_7$ below $T_N = 155$ K consists of an antiferromagnetic alignment of the iron moments along [001] [5]. No additional information regarding the structure or properties of the compound has been published to date. Here, the crystal and electronic structures of $La_3Fe_2S_7$ are reported. Furthermore, the physical properties of the compound on the basis of Mößbauer spectra, the magnetic susceptibility and the electrical resistivity are discussed.

* Corresponding author. Fax: +49 351 463 37287.
E-mail address: Michael.Ruck@chemie.tu-dresden.de (M. Ruck).

0022-4596/$ - see front matter © 2009 Elsevier Inc. All rights reserved.
doi:10.1016/j.jssc.2009.01.035

2. Experimental

2.1. Synthesis and chemical analysis

Crystals of $La_3Fe_2S_7$ were isolated from a reaction of the elements in an alkali metal chloride flux. Starting reactants were lanthanum (pieces, 99.9%, TBL-Kelpin; freshly filed under argon), iron (powder, 99.99%, ABCR; treated with H_2 at 770 K), and sulfur (powder, >99%, VEB Laborchemie; recrystallized from CS_2, then purified of carbon according to the method of *von Wartenberg* [6]). A 1:1 mixture of LiCl (p. a., Merck) and KCl (p. a., J.T. Baker), which was first heated under dynamic vacuum to remove any moisture, was used as a flux. The elements lanthanum, iron, and sulfur, in a ratio of 3:2:7 (0.5 g in total), were combined with the LiCl/KCl flux (1 g) in a fused-silica ampoule (12 cm length, 1.5 cm diameter), which was then sealed under vacuum (0.1 Pa). The reaction mixture was heated at 970 K for 14 days and then cooled to room temperature at a rate of 100 K h^{-1}. The flux was removed by washing the sample several times with water and ethanol. The major component of the product was $La_3Fe_2S_7$, which forms as black hexagonal prisms. The composition of the crystals was determined by energy-dispersive X-ray (EDX) analyses on a CamScan CS44 scanning electron microscope: La 26(1), Fe 15.2(2), S 59(2) mol% (average of two analyses); expected: La 25, Fe 16.7, S 58.3 mol%.

Powder samples of $La_3Fe_2S_7$ could also be prepared by heating oxides of the metals in a stream of H_2S, as reported previously [1,7]. A stoichiometric mixture (1 g in total) of La_3O_2 (powder, 99.98%, Fluka) and Fe_2O_3 (powder, 99%, Riedel-de-Haen) was placed in a glassy carbon boat contained in a fused-silica reactor. The reaction mixture was heated at 970 K under flowing H_2S (Messer Griesheim) for 6 h. Powder X-ray diffraction analysis on a Siemens D5000 diffractometer indicated the presence of a small amount of $La_{10}S_{14}O$ (ca. 10%), in addition to the major phase, $La_3Fe_2S_7$, but no detectable iron-containing impurities. Since no single-phase samples could be obtained in bulk quantity, all the subsequent physical characterization has been carried out with this polycrystalline sample.

2.2. X-ray structure determination

Intensity data for a single crystal of $La_3Fe_2S_7$ were collected at 293 K using graphite-monochromated Mo-$K\alpha$ radiation on a Stoe IPDS-II imaging plate diffractometer. Crystal data and further details of the data collection are given in Table 1. A numerical absorption correction, based on a crystal description optimized using equivalent reflections with X-SHAPE [8], was applied with the program X-RED [9]. The atomic coordinates of $Ce_3Fe_{1.94}S_7$ [3] and the hexagonal space-group $P6_3$ (no. 173) were used as an initial model for the structure, which was then refined on F^2 using SHELXL97 [10]. All atoms were refined with anisotropic displacement parameters. Despite the polarity of the space group, inversion twinning was not observed. Since the displacement ellipsoid of Fe(2) was initially unusually large, the occupancy of the octahedral iron site was refined freely. The resulting formula was $La_3Fe_{1.958(6)}S_7$, consistent with the EDX analyses. Final values of the positional and displacement parameters are given in Tables 2 and 3. Selected interatomic distances are listed in Table 4. Further data, in the form of a CIF, have been deposited with the Fachinformationszentrum Karlsruhe, 76344 Eggenstein-Leopoldshafen, Germany (E-mail address: crysdata@fiz-karlsruhe.de), as supplementary material no. 420072 and can be obtained by contacting the FIZ (quoting the article details and the corresponding CSD number). Graphics were prepared using the program Diamond [11].

Table 1
Crystallographic data and details of the structure determination for $La_3Fe_{2-\delta}S_7$.

Formula	$La_3Fe_{1.958(6)}S_7$
Formula weight	750.45 g/mol
Crystal system, space group	Hexagonal, $P6_3$ (no. 173)
Cell parameters	$a = 10.1906(6)$, $c = 5.9543(4)$ Å, $V = 535.50(6)$ Å^3
Formula units per cell	$Z = 2$
Calculated density	$\rho_{calc} = 4.65$ g cm^{-3}
Crystal dimensions	$0.15 \times 0.15 \times 0.15$ mm^3
Temperature	293(1) K
Measurement device	Imaging-plate diffractometer (Stoe IPDS-II)
Radiation	Graphite-monochromated Mo–$K\alpha$ ($\lambda = 0.71073$ Å)
Measurement limits	$8.00 \leqslant 2\theta \leqslant 69.98^\circ$ $-16 \leqslant h \leqslant 16$, $-16 \leqslant k \leqslant 16$, $-9 \leqslant l \leqslant 9$
Scan type	$0 \leqslant \omega \leqslant 180^\circ$, $\Delta\omega = 1^\circ$; $\phi_1 = 0$, $\phi_2 = 35^\circ$
Absorption correction	Numerical, on the basis of a crystal description optimized using equivalent reflections [8,9]
Absorption coefficient	μ(Mo–$K\alpha$) = 156 cm^{-1}
Transmission factors	0.214–0.304
Number of reflections	11 089 measured, 1563 independent
Data averaging	$R_{int} = 0.045$, $R_\sigma = 0.018$
Structure refinement	Full-matrix least squares on F_o^2 [10]; anisotropic displacement parameters
Extinction parameter	0.0257(7)
Flack parameter	0.01(2)
Number of parameters, restraints	39, 1
Residual electron density	−0.98, +1.26 e Å^{-3}
Figures of merit	R_1 (all 1563 F_o) = 0.022 R_1 (1554 $F_o > 4\sigma(F_o)$) = 0.022 wR_2 (all 1570 F_o^2) = 0.050
Goodness of fit	$S = 1.19$

Table 2
Wyckoff positions, atomic coordinates and equivalent isotropic displacement parameters for $La_3Fe_{2-\delta}S_7$.

Atom	Wyck.	x	y	z	U_{eq}/(10^{-4} Å^2)
La	6*c*	0.37447(2)	0.14100(2)	0.22767(5)	101.1(6)
Fe(1)	2*b*	1/3	2/3	0.1444(2)	93(2)
Fe(2)	2*a*	0	0	0.0002(2)	125(3)
S(1)	6*c*	0.1451(1)	0.2332(1)	0.2554(2)	102(2)
S(2)	6*c*	0.5799(1)	0.0980(1)	0.5044(2)	102(2)
S(3)	2*b*	1/3	2/3	0.5189(3)	101(3)

The occupancy of the Fe(2) position is 0.958(6). The U_{eq} values are defined as one-third of the trace of the orthogonalized U_{ij} tensor.

Table 3
U_{ij}/(10^{-4} Å^2) coefficients of the tensors of the anisotropic displacement parameters of the form exp{$-2\pi^2[U_{11}h^2a^{*2}+\cdots+2U_{23}klb^*c^*]$}.

Atom	U_{11}	U_{22}	U_{33}	U_{12}	U_{13}	U_{23}
La	82.6(8)	104.9(9)	115.9(9)	46.9(6)	15.6(9)	20.4(9)
Fe(1)	105(2)	105(2)	70(3)	52(1)	0	0
Fe(2)	120(3)	120(3)	136(5)	60(2)	0	0
S(1)	91(3)	107(3)	116(4)	56(3)	17(3)	8(3)
S(2)	117(4)	100(3)	103(3)	64(3)	2(3)	8(3)
S(3)	113(4)	113(4)	76(5)	57(2)	0	0

2.3. Mößbauer spectroscopy

^{57}Fe Mößbauer spectra of a powder sample of $La_3Fe_2S_7$ mixed with sugar (such that the concentration of iron was 5–10 mg cm^{-3}) were recorded at 300 and 78 K on a noncommercial apparatus consisting of a linear arrangement of source, absorber and detector. Transmission spectra were measured over 30 h with

Table 4
Selected interatomic distances (/Å) for $La_3Fe_2S_7$.

La–S(2)	2.865(1)	Fe(1)–S(3)	2.230(2)
La–S(3)^{i}	2.9011(7)	Fe(1)–S(2)^{i}, S(2)^{vii}, S(2)^{viii}	2.260(1)
La–S(1)^{ii}	2.9215(9)	Fe(1)···S(3)^{ix}	3.724(2)
La–S(1)	2.9274(9)		
La–S(2)^{iii}	2.963(1)	Fe(2)–S(1)^{v}, S(1)^{viii}, S(1)^{x}	2.539(1)
La–S(2)^{iv}	3.008(1)	Fe(2)–S(1), S(1)^{ii}, S(1)^{xi}	2.575(1)
La–S(1)^{v}	3.081(1)	Fe(2)···Fe(2)^{x}, Fe(2)^{xii}	2.9771(2)
La–S(1)^{vi}	3.386(1)		

Symmetry operations: (i) $1-x, 1-y, -1/2+z$; (ii) $-x+y, -x, z$; (iii) $1-x+y, 1-x, z$; (iv) $1-x, -y, -1/2+z$; (v) $y, -x+y, -1/2+z$; (vi) $y, -x+y, 1/2+z$; (vii) $y, 1-x+y, -1/2+z$; (viii) $x-y, x, -1/2+z$; (ix) $x, y, -1+z$ (x) $-x, -y, -1/2+z$; (xi) $-y, x-y, z$; (xii) $-x, -y, 1/2+z$.

a ^{57}Co source in a rhodium matrix, using α-Fe as a standard. The spectra were fit with transmission integrals.

2.4. Magnetic measurements

Magnetic-susceptibility measurements were made on powder samples of $La_3Fe_2S_7$ (ca. 50 mg), using a Quantum Design MPMS XL-7 SQUID magnetometer. The sample magnetization was measured over a temperature range of 1.8–400 K in magnetic fields up to $\mu_0 H = 7$ T.

2.5. Electrical resistivity

Electrical-resistivity measurements were made on a cold pressed-powder pellet with four-point contacting over the temperature range from 4 to 320 K, using a Quantum Design PPMS 9. Below about 170 K, the resistance of the sample was too high to be measured with the ac transport option of the instrument. Magnetoresistivity measurements were made in magnetic fields up to $\mu_0 H = 9$ T.

2.6. Quantum-chemical calculations

A full-potential non-orthogonal local-orbital calculation scheme (FPLO) [12] within the LDA was applied to obtain detailed insight into the electronic structure. In the scalar-relativistic calculations the exchange and correlation potentials of Perdew and Wang [13] were used. As the basis set, La(4*f*, 5*s*, 5*p*, 6*s*, 6*p*, 5*d*), Fe(3*s*, 3*p*, 4*s*, 4*p*, 3*d*) and S(2*s*, 2*p*, 3*s*, 3*p*, 3*d*) states were employed. The lower lying states were treated fully relativistically as core states. The S 3*d* states were taken into account as polarization states to increase the completeness of the basis set. The treatment of the La(4*f*, 5*s*, 5*p*), Fe(3*s*, 3*p*) and S(2*s*, 2*p*) semi-core like states as valence states was necessary to account for non-negligible core–core overlaps. The spatial extension of the basis orbitals, controlled by a confining potential $(r/r_0)^4$, was optimized to minimize the total energy [14]. A *k*-mesh of 312 points in the irreducible part of the Brillouin zone (1728 in the full zone) was used to ensure accurate density of states (DOS) and band structure information, especially in the region close to the Fermi level.

3. Results and discussion

$La_3Fe_2S_7$ is a member of a large family of chalcogenides of composition $R_3MM'Q_7$, where *R* is a rare-earth metal, *M* and *M*′ are metals or metalloids in tetrahedral and octahedral sites, respectively, and *Q* is sulfur or selenium [7,15]. The $Ce_6Al_{10/3}S_{14}$ structure type adopted by these compounds has been discussed previously

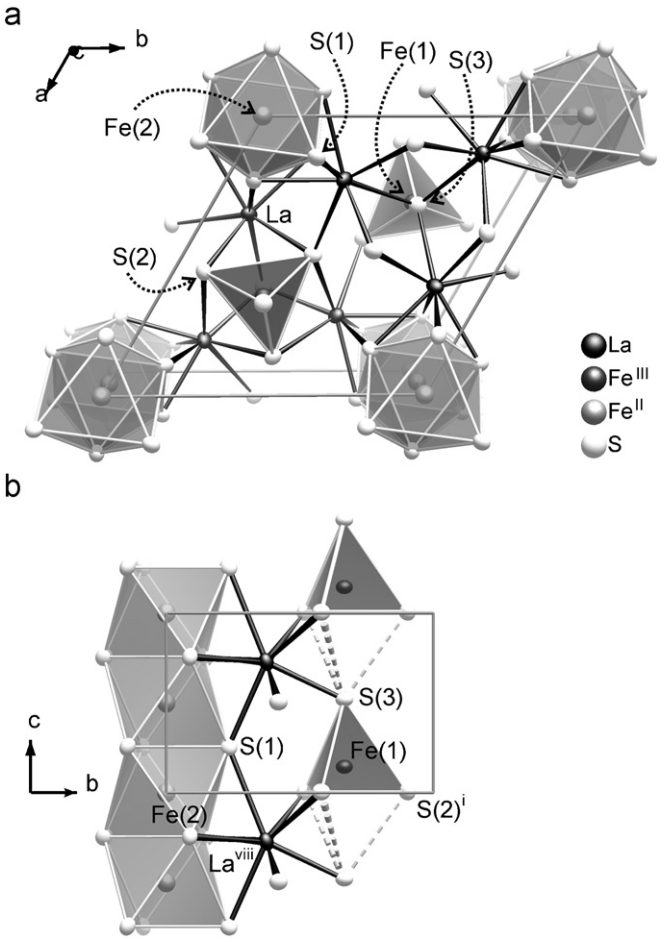

Fig. 1. Views of the $La_3Fe_2S_7$ structure: (a) along [001] and (b) along [100], highlighting the iron-centered tetrahedra and octahedra. Displacement ellipsoids are drawn at the 95% probability level. See Table 4 for symmetry operations.

[2,3], but the essential features of the $La_3Fe_2S_7$ structure will be summarized here to facilitate the interpretation of the electronic structure. In $La_3Fe_2S_7$, iron cations occupy both the tetrahedral sites *M* (Fe(1)) and the octahedral sites *M*′ (Fe(2)). The two types of coordination polyhedra are highlighted in views of the crystal structure along [001] and [100] presented in Fig. 1.

Stacks of $Fe^{III}S_4$ tetrahedra, all pointing in the polar [001] direction, lie on the threefold rotation axes of the cell (Fig. 1b). The Fe(1)–S(2) and Fe(1)–S(3) distances of 2.260(1) and 2.230(2) Å within the $Fe(1)S(2)_3S(3)$ tetrahedra are similar to those occurring in the FeS_4 tetrahedra of Fe^{III} compounds, for example, $KFeS_2$ (2.232–2.238 Å) [16]. Alternatively, the stacks of tetrahedra may be viewed as chains of corner-sharing FeS_5 trigonal bipyramids, although the Fe(1)···S(2) distance of 3.724(2) Å between the central iron atom of one tetrahedron and the apical sulfur atom of the next tetrahedron in the stack is considerably longer than a typical bonding distance.

The $Fe^{II}S_6$ octahedra share opposite faces, generating rods that orient parallel to the 6_3 screw axis (Fig. 1b). The iron atoms within the $Fe(2)S(1)_6$ octahedra are located slightly off-center, at a distance of 2.539(1) Å to the three sulfur atoms of one shared face, and at a distance of 2.575(1) Å to those of the other. These distances are within the range observed in the FeS_6 octahedra of the Fe^{II} compound $La_2Fe_2S_5$ (2.45–2.67 Å) [17]. The Fe(2)···Fe(2) separation within the rods is $c/2 = 2.9771(2)$ Å. The almost spherical displacement ellipsoids give no indication for a distortion of the equidistant linear sequence of Fe^{II} atoms.

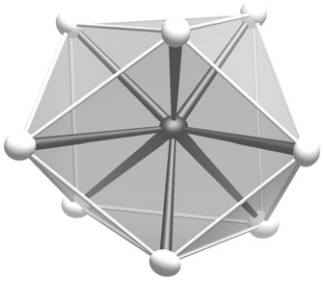

Fig. 2. Bicapped trigonal prismatic coordination of the La^{III} cations in $La_3Fe_2S_7$. Displacement ellipsoids are drawn at the 95% probability level. See Table 4 for symmetry operations.

The two types of chains of iron–sulfur polyhedra are connected by La^{III} cations. The lanthanum atoms are coordinated by [7+1] sulfur atoms in a bicapped trigonal prismatic arrangement: one S(3), three S(2) and three S(1) atoms at La–S distances of 2.865–3.081 Å, and an additional S(1) atom at a longer distance of 3.386(1) Å (Fig. 2). The shorter distances are within the range found in the LaS_8 bicapped trigonal prisms of $La_2Fe_2S_5$ (2.89–3.14 Å) [17].

The oxidation states of the iron cations can be estimated from the Fe–S bond lengths and coordination numbers of the Fe(1) and the Fe(2) sites. According to bond–valence theory [18], the valence V_i of an atom i corresponds to the sum of valences v_{ij} for all the bonds between atom i and atom j. The bond valences v_{ij} are determined from the empirical expression $v_{ij} = \exp\{(R_{ij}-d_{ij})/b\}$, involving the bond lengths d_{ij}, the bond–valence parameter R_{ij}, and the constant $b = 0.37$ Å. If a bond–valence parameter of $R_{FeS} = 2.16$ Å is used for Fe–S bonds, iron valences of $V_{Fe(1)} = 3.11$ and $V_{Fe(2)} = 2.06$ are calculated for the tetrahedral and octahedral sites, respectively. These values suggest that Fe^{III} cations occupy the Fe(1) site and Fe^{II} cations the Fe(2) site. The investigated single-crystal showed an iron deficiency of 2.1(3)%. The vacancies (symbolized with □) on the Fe(2) position are the consequence of a partial oxidation of Fe^{II} to Fe^{III}, according to the charge-balanced formula $(La^{III})_3(Fe^{III})_{1.084}(Fe^{II})_{0.874}\square_{0.042(6)}(S^{-II})_7$.

For further investigation of the valence state of the two types of iron cations in $La_3Fe_2S_7$ ^{57}Fe Mößbauer spectroscopy was applied. The spectra collected for $La_3Fe_{2-\delta}S_7$ at 300 and 78 K are presented in Fig. 3, and the parameters derived from these spectra are summarized in Table 5.

The Mößbauer spectrum recorded at 300 K consists of a singlet at an isomer shift of $\delta = 0.07(3)$ mm s^{-1} and a doublet at an isomer shift of $\delta = 0.96(4)$ mm s^{-1} with a quadrupole splitting of $\Delta E_Q = 0.78(8)$ mm s^{-1}. Upon comparison to the typical ranges of isomer shifts and quadrupole splittings, the singlet can be assigned to high-spin Fe^{III} cations, and the quadrupole doublet to high-spin Fe^{II} cations [19]. The presence of only two signals implies that the Fe^{III} and Fe^{II} cations each occupy a distinct coordination environment. Integration of the peak areas results in a Fe^{III}/Fe^{II} ratio of 54:46, which suggests that the fully occupied tetrahedral Fe(1) site contains Fe^{III} cations, and that the partially occupied octahedral Fe(2) site contains Fe^{II} cations. The composition $La_3(Fe^{III})_{1.06}(Fe^{II})_{0.91}\square_{0.03}S_7$ of the powder derived from the peak-area ratio of the Mößbauer experiments is in good agreement with the crystallographically determined composition of $La_3(Fe^{III})_{1.084}(Fe^{II})_{0.874}\square_{0.042(6)}S_7$ of the single crystal.

In the Mößbauer spectrum recorded at 77 K, hyperfine splitting occurs for both signals: a symmetric quadrupole sextet arising from a hyperfine field of $B_{HF} = 39.58(2)$ T is observed for the Fe^{III} cations, and an asymmetric quadrupole sextet arising from a hyperfine field of $B_{HF} = 19.35(2)$ T is observed for the Fe^{II} cations.

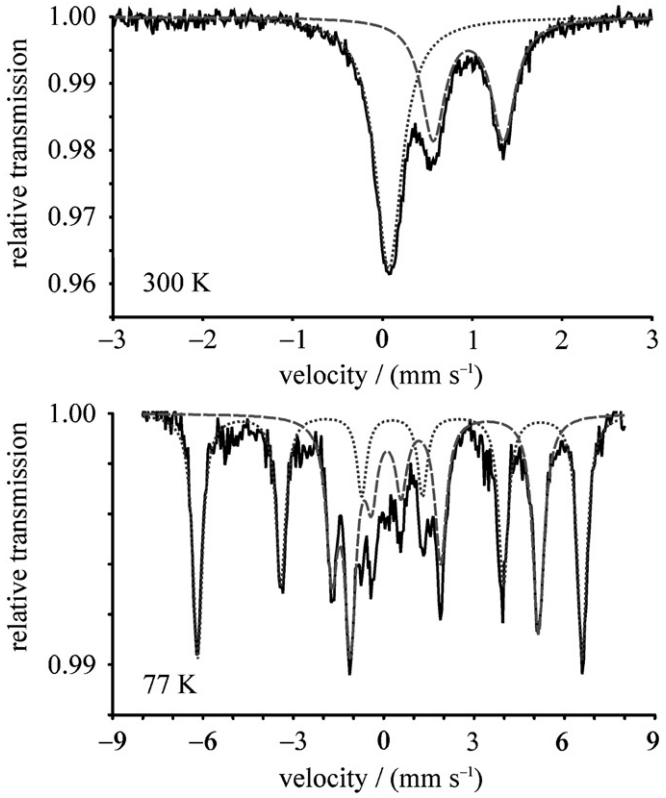

Fig. 3. ^{57}Fe Mößbauer spectra of $La_3Fe_{2-\delta}S_7$ at 300 and 77 K.

Table 5
Selected Mößbauer data for $La_3Fe_{2-\delta}S_7$.

T/K	Assignment	δ/(mm s^{-1})	ΔE_Q/(mm s^{-1})	B_{HF}/T	%
300	High-spin Fe^{III}	0.07(3)			54
	High-spin Fe^{II}	0.96(4)	0.78(8)		46
77	High-spin Fe^{III}	0.10(3)		39.58(2)	49
	High-spin Fe^{II}	0.91(4)	1.93(6)	19.35(2)	51

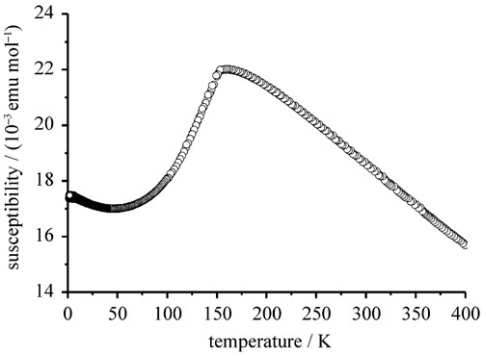

Fig. 4. Temperature dependence of the molar magnetic susceptibility of $La_3Fe_{2-\delta}S_7$ in a magnetic field of 7 T.

Although the complexity of the spectrum reduces the accuracy of the fitting, it is clear that magnetic ordering involving both types of iron cations occurs at 77 K, consistent with the reported antiferromagnetic structure of $La_3Fe_{2-\delta}S_7$ below $T_N = 155$ K [5].

The temperature dependence of the magnetic susceptibility χ of $La_3Fe_{2-\delta}S_7$ in a magnetic field of 7 T is shown in Fig. 4. An

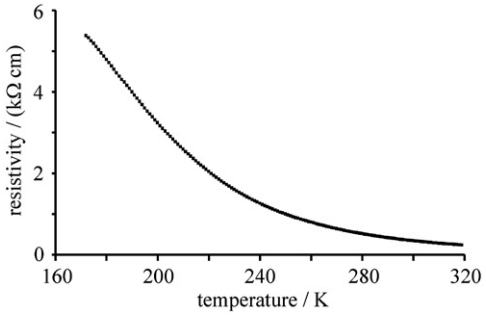

Fig. 5. Temperature dependence of the electrical resistivity of a pressed-powder pellet of $La_3Fe_{2-\delta}S_7$.

antiferromagnetic transition occurs at $T_N \approx 155$ K, in agreement with previous neutron diffraction experiments [5]. Above this temperature, paramagnetic behavior is observed. However, owing to the presence of a sizable amount of a ferromagnetic impurity (with $T_C > 400$ K), the susceptibility in the paramagnetic range is field dependent. Therefore, the Honda–Owen method (extrapolation of $\chi(H^{-1})$ to $H^{-1} \rightarrow 0$) was used to extract the contribution of $La_3Fe_{2-\delta}S_7$ from susceptibility data recorded at 3.5 and 7 T [20,21]. A fit of the corrected data over 250–400 K to the Curie–Weiss law yields an effective magnetic moment of $\mu_{eff} = 8.2\,\mu_B$, which is somewhat higher than the theoretical value of $\mu_{calc} = 7.7\,\mu_B$ calculated from the spin-only moments of high-spin Fe^{II} ($4.9\,\mu_B$) and Fe^{III} ($5.9\,\mu_B$) ions of the stoichiometric compound. The Weiss parameter of $\theta = -292$ K determined from the fit is consistent with strong antiferromagnetic exchange interactions.

The temperature dependence of the electrical resistivity $\rho(T)$ of the cold-pressed bar of $La_3Fe_{2-\delta}S_7$ over 170–320 K is shown in Fig. 5. The strong increase of $\rho(T)$ with decreasing T is typical for a thermally activated conduction mechanism. A standard plot of $\ln\sigma$ vs. T^{-1} displays, however, only an approximately linear behavior for the high-temperature regime $250\,K < T < 320\,K$. The slope corresponds to a small semiconductor band gap of $E_g = 0.3$ eV, which should be understood as a minimum value due to the extended defects. Nevertheless, at 293 K the resistivity is quite large ($\rho_{293\,K} \approx 4\,\Omega$ m).

In contrast to the observations, the electronic structure of the compound (see below) suggests a metal-like conduction of charge carriers. In view of the defects of Fe in the metallic structural units a hopping-type conduction mechanism may be considered. We therefore tried to fit $\rho(T)$ for $250\,K < T < 320\,K$ with a variable range hopping [22] in one, two and three dimensions d. A better fit than for a fixed-gap semiconductor is obtained for all choices of d, the best fit, however, is observed for three-dimensional hopping, which gives the weakest temperature variation. In that respect $La_3Fe_{2-\delta}S_7$ behaves similar to the $(Ca_7N_4)[M_x]$ (M = Ag, Ga, In, Tl) compounds [23], which have linear metallic chains as guests in channels of a subnitride host. On polycrystalline samples of these compounds, resistivity measurements also showed variable range hopping conduction with $d = 3$, in spite of the one-dimensional character of the metallic structural units. Resistivity measurements on $La_3Fe_{2-\delta}S_7$ in a magnetic field of $\mu_0 H = 9$ T did not reveal any significant magnetoresistance.

The resulting DOS is shown in Fig. 6. The low-lying part of the valence band (between −5.5 and −1.5 eV) is dominated by sulfur 3p contributions with an admixture from Fe and La. The band complex at the Fermi level (between −1.5 and 1 eV) is dominated by Fe 3d states. Whereas the S contributions to the valence band are quite similar, the Fe states are clearly distinct according to the tetrahedral Fe^{III}_{tet} and octahedral Fe^{II}_{oct} positions. In Fig. 7 the Fe 3d related bands close to the Fermi level are depicted with respect to the Fe site (upper panel: Fe_{oct}; lower panel: Fe_{tet}) and their orbital

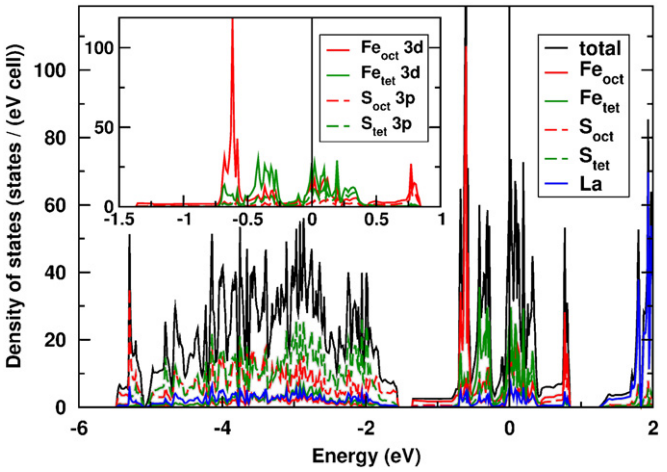

Fig. 6. Total and partial electronic density of states for $La_3Fe_2S_7$. The partial contributions are shown according to the octahedral (oct) Fe^{II} and tetrahedral (tet) Fe^{III} sites. The inset shows the contribution of Fe 3d and S 2p states for the octahedral and tetrahedral sites close to the Fermi level, which is set to zero energy.

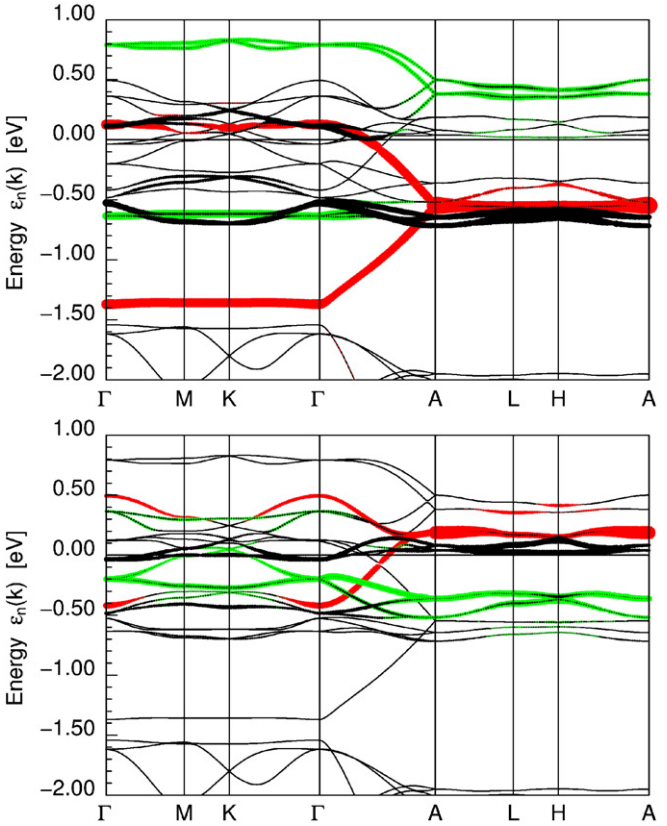

Fig. 7. Band structure and Fe 3d "fat bands" for $La_3Fe_2S_7$ close to the Fermi level, which is set to zero energy. The upper panel shows the Fe 3d characters ($3d_{3z^2-r^2}$—red, $3d_{xz,yz}$—green, $3d_{x^2-y^2,xy}$—black) for the octahedral site and the lower panel for the tetrahedral site, respectively. For interpretation of the references to color in this figure legend , the reader is referred to the web version of this article.

character ($3d_{xy,yz}$; $3d_{xy,x^2-y^2}$; $3d_{z^2-r^2}$). Comparing the upper panel and the lower panel of figure Fig. 7, the considerable narrower band width of the Fe_{tet} bands is obvious. This can be understood due to the isolated nature of the tetrahedra. In contrast, the Fe_{oct} are linked by S atoms, resulting in a larger dispersion. This is also

visible in the DOS in the inset of Fig. 6. A closer look at the Fe 3*d* bands reveals that the main dispersion for both Fe sites is along the hexagonal axis, carried by the $3d_{z^2-r^2}$ orbitals. These bands show a quasi one-dimensional characteristic with a small dispersion in the hexagonal plane, only. The dispersions of all other Fe 3*d* related bands are comparably small. The quasi one-dimensional nature of the Fe_{oct} $3d_{z^2-r^2}$ bands along the hexagonal axis is also reflected in the DOS, forming van Hove singularities at about −0.7 and 0.75 eV. Furthermore, Fig. 7 reveals that the interaction (mixing) between the two Fe species is quite small and limited to a small region of the *k*-space, only.

For the origin of the discrepancy between the experimentally observed activated behavior and the metallic character according to the band structure calculations two possible explanations can be provided: (i) The band dispersion and therefore the related transport properties have strong one-dimensional character along the hexagonal axis. For an un-oriented powder sample, this leads to a drastically reduced conductivity, depending on the grain boundaries. Furthermore, the presence of iron vacancies reduces the number of valence electrons. In a rigid band approximation, this lowers the Fermi level so that it falls into the pseudo gap at about −0.1 to −0.2 eV (see Figs. 6 and 7), resulting in a drastic reduction of the DOS at the Fermi energy and a further reduced conductivity. (ii) Similar to transition metal oxides, the covalency between Fe and S will cause strong or intermediate electron correlations, resulting in further localization of the Fe 3*d* related charge carriers. This effect is, according to common experience, not well described by LDA calculations. Since the charge carriers at the Fermi level are predominantly Fe 3*d* electrons, such correlations will additionally suppress the metallic character of the compound. For a quantitative study of correlation effects in the Fe 3*d* shell, a sophisticated treatment using the LDA+DMFT technique seems to be a precondition to cover the dynamic nature of these correlations. A static treatment of the correlations using the mean field like LDA+*U* method did not improve the results with respect to the metallic behavior.

Acknowledgments

We gratefully acknowledge the experimental help of Ms. J. Krug and the financial support of the Deutsche Forschungsgemeinschaft (DFG) within the SFB 463.

References

[1] G. Collin, F. Rouyer, J. Loriers, C. R. Acad. Sci. Ser. C 266 (1968) 689–691.
[2] D. de Saint-Giniez, P. Laruelle, J. Flahaut, C. R. Acad. Sci. Ser. C 267 (1968) 1029–1032.
[3] A.M. Mills, M. Ruck, Acta Crystallogr. Sect. C 60 (2004) i71–i72.
[4] Z.S. Gönen, P. Fournier, V. Smolyaninova, R. Greene, F.M. Araujo-Moreira, B. Eichhorn, Chem. Mater. 12 (2000) 3331–3336.
[5] R. Plumier, M. Lecomte, G. Collin, F. Keller-Besrest, Phys. Lett. Sect. A 76 (1980) 419–420.
[6] H. von Wartenberg, Z. Anorg. Allg. Chem. 286 (1956) 243–246.
[7] J. Flahaut, P. Laruelle, in: L. Eyring, M. O'Keeffe (Eds.), The Chemistry of Extended Defects in Non-Metallic Solids, North-Holland, Amsterdam, 1970, pp. 109–123.
[8] X-SHAPE 1.06, Program for crystal optimization for numerical absorption correction, STOE & Cie, Darmstadt, 1999.
[9] X-RED 1.22, Program for data reduction, STOE & Cie, Darmstadt, 2001.
[10] G.M. Sheldrick, Acta Crystallogr. Sect. A 64 (2008) 112.
[11] K. Brandenburg, Diamond 3.1f, Visual crystal structure information system, Crystal Impact, Bonn, 2008.
[12] K. Koepernik, H. Eschrig, Phys. Rev. B 59 (1999) 1743.
[13] J.P. Perdew, Y. Wang, Phys. Rev. B 45 (1992) 13244.
[14] H. Eschrig, Optimized LCAO Method and the Electronic Structure of Extended Systems, Springer, Berlin, 1989.
[15] P. Villars, Pearson's Handbook Desk Edition, ASM International, Materials Park, Ohio, 1997.
[16] A.K. Pant, E.D. Stevens, Phys. Rev. B 37 (1988) 1109–1120.
[17] F. Besrest, G. Collin, J. Solid State Chem. 21 (1977) 161–170.
[18] N.E. Brese, M. O'Keeffe, Acta Crystallogr. Sect. B 47 (1991) 192–197.
[19] D. Barb, Grundlagen und Anwendungen der Mößbauer-Spektroskopie, Akademie, Berlin, 1980.
[20] K. Honda, Ann. Phys. (Leipzig) 32 (1910) 1027.
[21] H. Lueken, Magnetochemie, Teubner, Stuttgart, 1999.
[22] N.F. Mott, Phil. Mag. 19 (1969) 835.
[23] P. Höhn, G. Auffermann, R. Ramlau, H. Rosner, W. Schnelle, R. Kniep, Angew. Chem. 118 (2006) 6833–6837;
P. Höhn, G. Auffermann, R. Ramlau, H. Rosner, W. Schnelle, R. Kniep, Angew. Chem. Int. Ed. 45 (2006) 6681–6685.